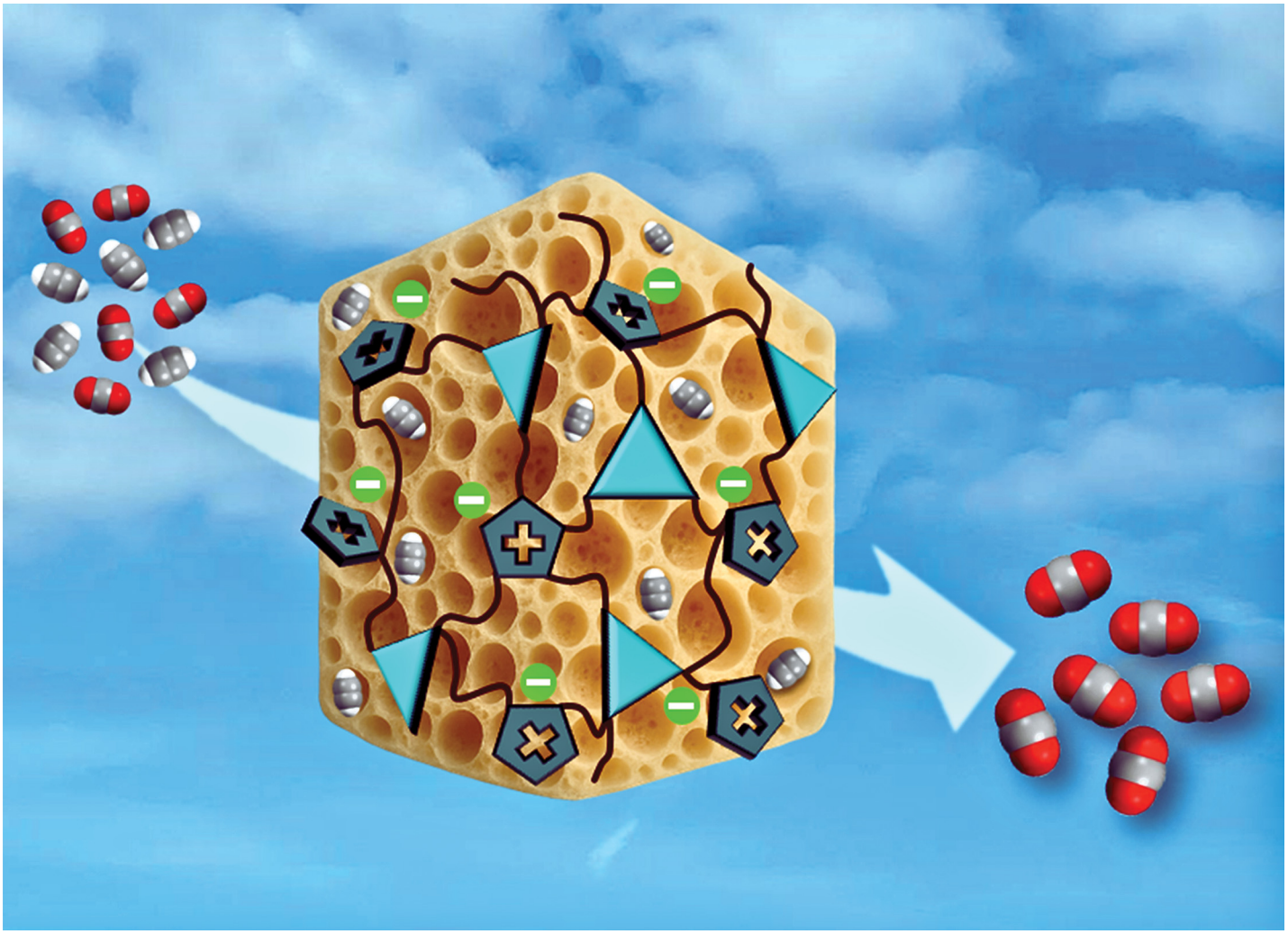

Showcasing research from Professor Soumya Mukherjee's laboratory, Department of Chemical Sciences and The Synthesis and Solid State Pharmaceutical Centre (SSPC), University of Limerick, Ireland.

An ionic ultramicroporous polymer with engineered nanopores enables enhanced acetylene/carbon dioxide separation

Engineered nanopores within ionic ultramicroporous polymers enable selective capture of acetylene (C_2H_2) over carbon dioxide (CO_2). Extending the cationic framework doubles the C_2H_2/CO_2 selectivity, offering a promising route for efficient light hydrocarbon separation.

Image reproduced by permission of Soumya Mukherjee from *Chem. Commun.*, 2025, **61**, 6466.

As featured in:

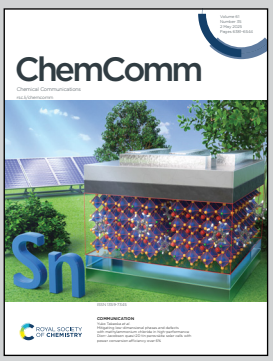

See Matthias Vandichel, Soumya Mukherjee *et al.*, *Chem. Commun.*, 2025, **61**, 6466.

ROYAL SOCIETY OF CHEMISTRY

rsc.li/chemcomm

Registered charity number: 207890

ChemComm

COMMUNICATION

View Article Online
View Journal | View Issue

Check for updates

Cite this: *Chem. Commun.*, 2025, **61**, 6466

Received 28th February 2025,
Accepted 26th March 2025

DOI: 10.1039/d5cc01092f

rsc.li/chemcomm

Open Access Article. Published on 27 March 2025. Downloaded on 1/26/2026 5:33:42 AM.
This article is licensed under a Creative Commons Attribution 3.0 Unported Licence.

An ionic ultramicroporous polymer with engineered nanopores enables enhanced acetylene/carbon dioxide separation†

Asif Raza, ‡[a] Sousa Javan Nikkhah, ‡[a] Lilia Croitor,[a] Ahmed Gamal Attallah, [bc] Eric Hirschmann, [b] Matthias Vandichel *[a] and Soumya Mukherjee *[a]

A nanopore engineering approach enhances acetylene (C_2H_2) over carbon dioxide (CO_2) selectivity in ionic ultramicroporous polymers (IUPs), an understudied class of sorbents. Extending the cationic arm of a prototypical IUP nearly doubles its C_2H_2/CO_2 selectivity from 4.9 to 8.5 (at 298 K, 1 bar), underpinned by further observations from dynamic separation experiments and bespoke computational insights.

Acetylene (C_2H_2) is a key industrial feedstock used in the production of plastics, pharmaceuticals, fuels, and other raw chemicals.[1] Traditionally, C_2H_2 is produced *via* methane combustion or petroleum cracking, processes that generate carbon dioxide (CO_2) as the primary impurity. The separation of these two gases is key to obtaining polymer-grade C_2H_2 ($\geq$99.5%), but their similar molecular sizes (kinetic diameters $\sim$ 3.3 Å), linear shapes, and close boiling points (189.2 K for C_2H_2 and 194.7 K for CO_2) make their separation highly challenging.[2] State-of-the-art processes still rely upon traditional purification methods, such as solvent extraction and cryogenic distillation, which are energy-intensive and inefficient, underscoring the need for more sustainable alternatives.[3–5]

Adsorptive separation, particularly physisorption, offers clear advantages because of its minimal energy demand for sorbent recycling (*i.e.*, regeneration).[6] Physisorbents that offer strong, selective binding for C_2H_2 over CO_2 appear particularly suited for the target C_2H_2/CO_2 separation.[6,7] Reticular crystalline physisorbents like porous coordination networks (PCNs), such as metal–organic frameworks (MOFs)[8] and hybrid ultramicroporous materials (HUMs),[9,10] and hydrogen bonded organic frameworks (HOFs)[11,12] have lately been developed for C_2H_2/CO_2 separation. Whereas high selectivity has been realised by a handful of such crystalline reticular sorbents, and the total number of crystalline CNs in the Cambridge Structural Database (CSD) is soaring above 100 000,[13] the labile nature of the metal–organic bonds/presence of metals have handicapped the performance benchmarks. With regard to chemical separations and/or purifications, such as light hydrocarbon separations, limited water stability has particularly kept the "spectrum of performance parameters" elusive for MOF physisorbents thus far.[6,14] Conversely, porous organic polymers (POPs), constructed from covalent bonds, tend to be stable under aqueous conditions, their physisorptive separation performances are poor because of two key factors that drive purifications in ultramicroporous PCNs, especially HUMs: (a) wrong pore size to enable tight binding, *i.e.*, ultramicroporosity (<7 Å); (b) inappropriate pore chemistry for selective binding between the adsorbent and target molecule. Crystalline POPs, as exemplified by covalent organic frameworks (COFs) suffer from these weaknesses despite their well-defined structures. For example, **NKCOF-12**, though capable of high acetylene (C_2H_2) uptake at 298 K, exhibits a modest C_2H_2/CO_2 selectivity (<5), limiting its applicability.[15] Amorphous POPs, such as porous aromatic frameworks (PAFs), offer high stability, scalability, and processability for membranes or monoliths, *etc.*, but fail to offer densely packed physisorption sites, *i.e.*, optimal combinations of pore size and chemistry key to strong and selective binding.

To overcome these oft-encountered limitations, ionic ultramicroporous polymers (IUPs), an advanced form of polyionic liquids (PILs)[16,17] that feature strong electrostatic functionalities and high stability have recently come to the fore.[5] However, the field is still in its infancy, with only a few reported examples and limited design principles for tailoring binding sites to selectively capture gases like C_2H_2, that could potentially afford binary C_2H_2/CO_2 separation performances. Among the handful of known IUPs, hitherto only one strategy, namely copolymerisation has been shown to improve the C_2H_2/CO_2 separation,[18] thanks to the

[a] *Department of Chemical Sciences, Bernal Institute and Research Ireland Centre for Pharmaceuticals (SSPC), University of Limerick, Limerick V94 T9PX, Ireland. E-mail: Matthias.Vandichel@ul.ie, Soumya.Mukherjee@ul.ie*
[b] *Helmholtz-Zentrum Dresden – Rossendorf, Institute of Radiation Physics, Bautzner Landstraße 400, 01328, Dresden, Germany*
[c] *Physics Department, Faculty of Science, Minia University, Minia 61519, Egypt*

† Electronic supplementary information (ESI) available. CCDC 2418964. For ESI and crystallographic data in CIF or other electronic format see DOI: https://doi.org/10.1039/d5cc01092f

‡ A. R. and S. J. N. contributed equally.

This journal is © The Royal Society of Chemistry 2025

Open Access Article. Published on 27 March 2025. Downloaded on 1/26/2026 5:33:42 AM.
This article is licensed under a Creative Commons Attribution 3.0 Unported Licence.

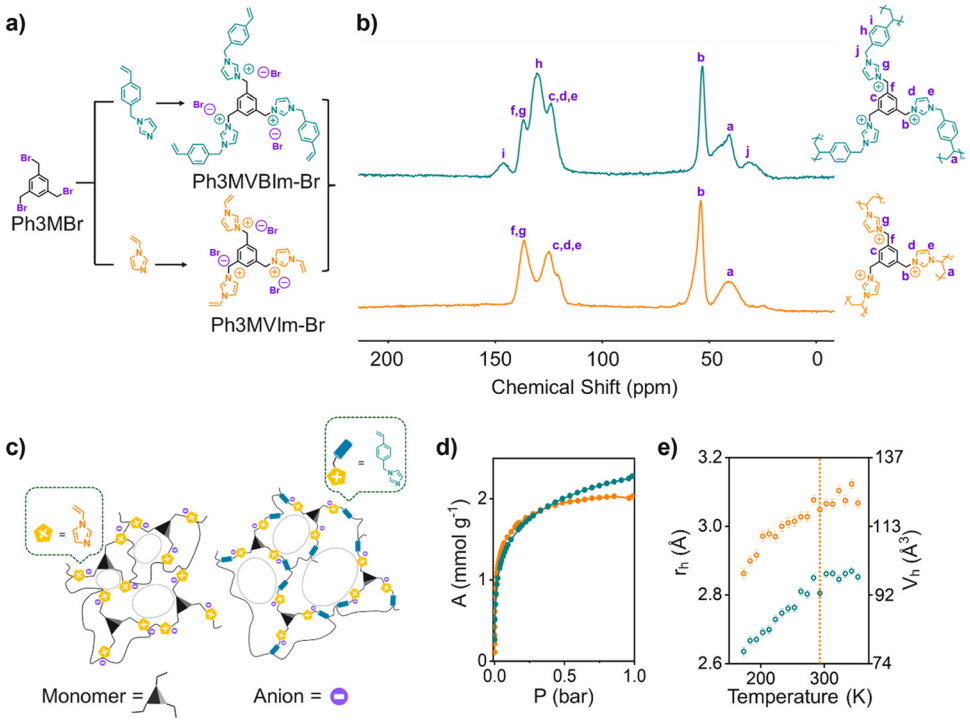

Fig. 1 (a) Synthesis scheme and chemical structures of the monomers; (b) solid-state ^{13}C NMR spectrum of **P(Ph3MVBIm-Br)** (green) and **P(Ph3MVIm-Br)** (orange); (c) schematic of the arm elongation strategy; (d) CO_2 adsorption isotherms for **P(Ph3MVBIm-Br)** (green) and **P(Ph3MVIm-Br)** (orange) at 195 K; (e) hole radii (r_h) and volumes (V_h) of the **P(Ph3MVBIm-Br)** (green) and **P(Ph3MVIm-Br)** (orange) from positron annihilation lifetime spectroscopy (PALS) experiment. The dotted line shows the results at room temperature of the as-synthesized sample.

authors controlling pore structure and functionality in **P(Ph3Im-Br-*n*DVB)** (Ph = phenyl, Im = vinylimidazolium cation, Br = bromide anion, DVB = divinylbenzene crosslinker, *n* = molar ratio of monomer and crosslinker). **P(Ph3Im-Br-0.5DVB)** registered a C_2H_2/CO_2 selectivity of 17.9 at 1 bar and 298 K, highlighting the necessity for further iteration of the IUP platform. Such compositional control in IUPs is likely to enable an improved, high-density distribution of the desired C_2H_2 binding sites. Herein, we report a nanopore engineering strategy by looking at IUPs as a tripartite composition, *i.e.*, a neutral central core (usually aromatic ring), cationic arm (having quaternized nitrogen) and counteranion. In this report, we have modulated the cationic arm by extending it with addition of an aromatic benzyl ring (Fig. 1a). This extended arm helped in almost doubling the selectivity from 4.9 for **P(Ph3MVIm-Br)** (Ph = phenyl, VIm = vinylimidazole, Br = bromide anion) to 8.5 for **P(Ph3MVBIm-Br)** (Ph = phenyl, VBIm = vinylbenzylimidazole, Br = bromide anion) at 1 bar and 298 K for equimolar mixtures of C_2H_2/CO_2.

IUPs were synthesized using a free radical polymerization technique, with detailed procedures provided in the ESI† (Fig. S1–S7). As shown in Fig. 1c, **P(Ph3MVBIm-Br)** features VBIm as its cationic arm, an extended version of VIm found in **P(Ph3MVIm-Br)**. During polymerization, the vinyl groups crosslinks, forming a porous structure. Solid-state NMR highlights differences between the polymers. **P(Ph3MVBIm-Br)** exhibits additional aliphatic signals at ~30 ppm (CH_2 groups) and ~43 ppm (covalently linked vinyl carbons). Peaks at ~54 ppm correspond to methylene linkers, while ~124 ppm and ~138 ppm can be attributed to aromatic carbons in the phenyl core and substituted imidazolium carbons, respectively. Unique signals in the aromatic region (h) and (i) confirm the presence of the benzene ring in the cationic arm of **P(Ph3MVBIm-Br)** (Fig. 1b). FT-IR spectra indicate successful polymerization, as the C=C stretching band at 1650 cm^{-1} diminishes in the polymers (Fig. S6 and S7, ESI†).

The textural properties of the polymers were assessed *via* CO_2 adsorption isotherms at 195 K (Fig. 1d), with structural parameters summarized in Table S1 (Fig. S8–S11, ESI†). Horvath Kawazoe analysis (Fig. S8 and S10 inset, ESI†) indicated pore widths of 4–7 Å. Positron annihilation lifetime spectroscopy (PALS) provided further insights, showing average pore radii of 2.6–2.8 Å for **P(Ph3MVBIm-Br)** and 2.8–3.1 Å for **P(Ph3MVIm-Br)** (Fig. 1e), with *ortho*-positronium (*o*-Ps) lifetimes of 2.16 ns and 1.93 ns at 298 K, respectively (Fig. S12, ESI†). More details about PALS are provided in the ESI.† Thermogravimetric analysis (TGA) further demonstrated the excellent thermal stability of these materials, with an initial decomposition temperature of 290 °C under a nitrogen atmosphere (Fig. S13 and S14, ESI†). The surface chemical properties of **P(Ph3MVBIm-Br)** were analysed using X-ray photoelectron spectroscopy (XPS) (Fig. S15, ESI†). XPS detected carbon, nitrogen, oxygen, and bromine, with their percentage abundances detailed in Table S2 (Fig. S15a, ESI†). High-resolution spectra revealed three distinct C 1s peaks at 284.5 eV (aromatic and cross-linked carbons), 285.6 eV (C–N bonds in imidazole rings), and 286.6 eV (C–O bonds, can be attributed to the presence of

Open Access Article. Published on 27 March 2025. Downloaded on 1/26/2026 5:33:42 AM.
This article is licensed under a Creative Commons Attribution 3.0 Unported Licence.

methanol solvent) (Fig. S15c, ESI†). N 1s spectra showed peaks at 399.3 eV (non-quaternized nitrogen) and 401.4 eV (quaternized nitrogen), confirming the polymer's cationic backbone (Fig. S15b, ESI†). Br 3d signals at 67.2 and 68.2 eV validated the presence of bromide anions as charge-balancing counterions (Fig. S15d, ESI†).

To evaluate the properties of IUPs in acetylene purification, adsorption isotherms of C_2H_2 and CO_2 were determined, revealing superior C_2H_2 uptake of 1.4 mmol g^{-1} **P(Ph3MVIm-Br)** and 1.0 mmol g^{-1} **P(Ph3MVBIm-Br)** at 298 K and 1 bar, with CO_2 uptakes significantly lower at 0.65 mmol g^{-1} and 0.4 mmol g^{-1} (Fig. 2a and b). The IAST selectivity for C_2H_2/CO_2 mixtures improved from 4.96 to 8.49 upon extending the cationic arm (Fig. 2c and Fig. S16, S17, ESI†), surpassing many porous organic polymers *e.g.*, ZJUT-3 (3.2),[19] NKCOF-12 (4.0),[15] and 3D pts COF (3.8)[20] (Fig. 2d and Table S3, ESI†). Adsorption data at 273 K and 283 K showed higher C_2H_2 uptake and a stronger binding affinity (Q_{st} = 46.7 kJ mol^{-1} for C_2H_2 *vs.* 39.7 kJ mol^{-1} for CO_2), (Fig. S18–S22 and Table S4, ESI†) affirming effective separation. The higher S_{AC} for **P(Ph3MVBIm-Br)** *vs.* **P(Ph3MVBIm-Br)** (Fig. 2c) is found to be in contrast with the significantly higher C_2H_2 uptake registered by the latter (1.4 mmol g^{-1}) over the former (1.0 mmol g^{-1}). Upon closely looking at the CO_2 isotherms' differences, particularly under low pressures, the weaker CO_2 affinity for **P(Ph3MVBIm-Br)** turns out to be the key behind its higher S_{AC}.

The realization of **P(Ph3VBIm-Br)** for challenging C_2H_2/CO_2 separation highlights the potential of IUPs in industrial applications. We further assessed its performance under ambient conditions by conducting laboratory-scale dynamic column breakthrough (DCB) experiments. Equimolar C_2H_2/CO_2 mixtures were passed through a packed column of activated **P(Ph3MVBIm-Br)** at 1 bar and 298 K. This showed delayed C_2H_2 breakthrough (24.33 min g^{-1}) compared to CO_2 (13.54 min g^{-1}), yielding a separation factor of 4.07 and a CO_2 purity of 99.12% during separation (Fig. 2e). Temperature-programmed desorption (TPD) confirmed facile regeneration at 60 °C, with high-purity fuel-grade C_2H_2 (>98%) eluted over 2.55–21.49 min g^{-1} and laboratory-grade C_2H_2 (>99%) eluted over 3.06–19.96 min g^{-1} (Fig. S23, ESI†). The peak C_2H_2 purity was 99.57%, with productivity reaching 1.53 L kg^{-1} for fuel-grade and 1.34 L kg^{-1} for lab-grade C_2H_2, demonstrating the material's industrial potential.

To gain insight into the mechanism underlying the separation performance, we conducted Canonical Monte Carlo (CMC) simulations using the crystallographic structure of the **Ph3MVIm-Br** monomer as the basis (Table S5, ESI†). For molecular models of **P(Ph3MVIm-Br)** and **P(Ph3MVBIm-Br)**, the CMC simulations at 298 K revealed that the C_2H_2 and CO_2 binding sites are located on the polymer surfaces (Fig. S32 and S33, ESI†). This surface-reliant binding is attributed to the morphology and high density of the polymers (Table S8, ESI†). Br^- ions afford a shielding layer on the surface (Fig. S30, ESI†), eliciting an electronegative environment that strongly interacts with C_2H_2 and CO_2, both polarizable in nature. Conversely, the Br^- ions limit diffusion into the dense interior (Fig. S30 and S31, ESI†).

Isosurface analyses, colour-mapped along potential energy (Fig. 3), revealed that C_2H_2 has the most favourable binding site on the surface, indicated by its lowest potential energy (Fig. 3a and c). This is driven by C_2H_2's high polarizability, electron-rich triple bond, and acetylenic hydrogens with p*K*a ~25, enabling

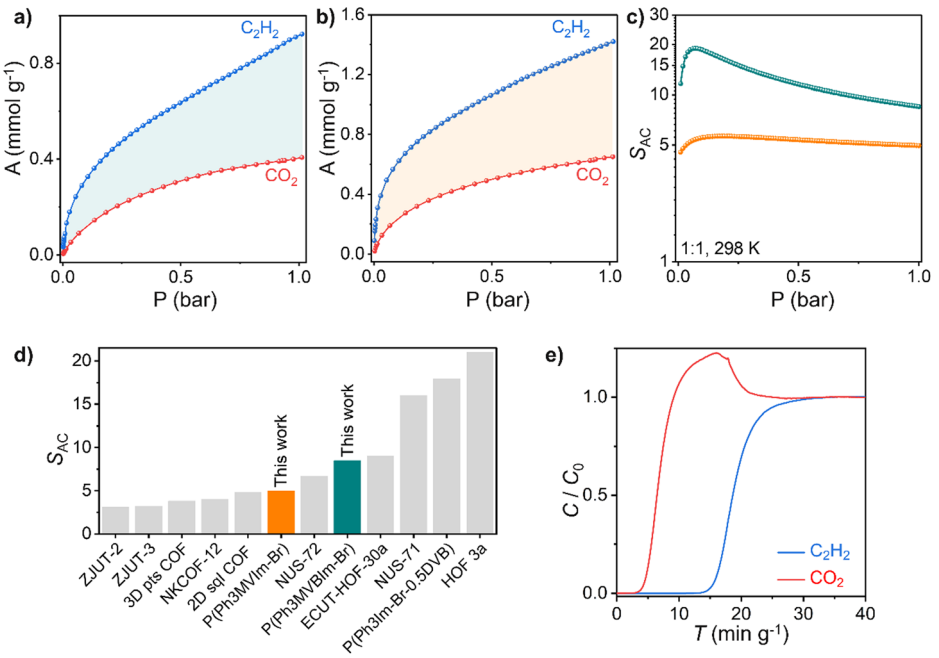

Fig. 2 (a) C_2H_2 and CO_2 adsorption isotherms on **P(Ph3MVBIm-Br)** at 298 K; (b) C_2H_2 and CO_2 adsorption isotherms on **P(Ph3MVIm-Br)** at 298 K; (c) IAST selectivities of a C_2H_2/CO_2 (S_{AC}) (1 : 1) mixture for the IUPs at 298 K (turquoise: **P(Ph3MVBIm-Br)**, and orange: **P(Ph3MVIm-Br)**); (d) comparison of IAST selectivities of the C_2H_2/CO_2 (1 : 1) mixture for porous organic polymers at 298 K, 1 bar; (e) dynamic column breakthrough profile recorded at 298 K for the C_2H_2/CO_2 (1 : 1, *v*/*v*) mixture for **P(Ph3MVBIm-Br)**.

 This journal is © The Royal Society of Chemistry 2025

Open Access Article. Published on 27 March 2025. Downloaded on 1/26/2026 5:33:42 AM.
This article is licensed under a Creative Commons Attribution 3.0 Unported Licence.

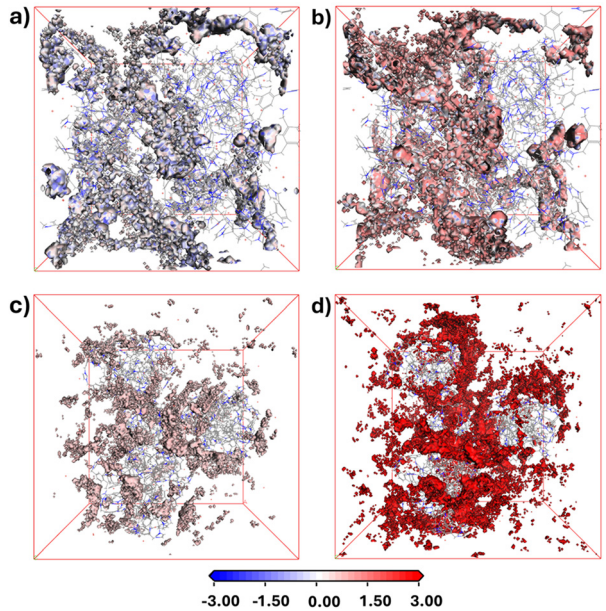

Fig. 3 Combined energy and density distribution information, coloured by potential energy of the adsorbate in kcal mol^{-1} of (a) **P(Ph3MVIm-Br)** for C_2H_2 and (b) CO_2; (c) **P(Ph3MVBIm-Br)** for C_2H_2 and (d) CO_2.

strong electrostatic and dipole interactions with the cationic backbone and the anionic Br^-. In contrast, CO_2 (Fig. 3c and d), with lower polarizability and no hydrogens, interacts weakly with the polymer surface, resulting in weak binding. Adsorbate binding density analysis revealed that **P(Ph3MVIm-Br)** features a higher density of binding sites for both C_2H_2 and CO_2 (Fig. S32, ESI†) *vs.* those in **P(Ph3MVBIm-Br)** (Fig. S33, ESI†), which leads to a higher uptake of both gases in **P(Ph3MVIm-Br)**. This is likely due to its compact structure, which may enhance adsorption through stronger dipole-quadrupole interactions between the closely packed imidazolium groups and the sorbate molecules. In **P(Ph3MVBIm-Br)**, an interplay of electrostatic interactions, steric hindrance from additional bulky phenyl groups, and the compact internal structure of the polymers further limits CO_2 adsorption (Fig. 3d), enhancing the selectivity for C_2H_2/CO_2.

Our findings demonstrate that tweaking the cationic arm of a prototypal IUP doubles the C_2H_2/CO_2 selectivity by limiting the CO_2 coadsorption. A detailed computational study reinforced the latter and further elucidated the importance of ionic surfaces in fostering strong binding sites, *vs.* the often-emphasised impact of pore voids and channels. It is therefore highly likely that next generation IUP sorbents will exhibit a high-density of ionic sites and abundant ultramicroporosity to address challenging separations.

Research Ireland awards (21/PATH-S/9454; 23/FFP-A/12221), SSPC Research Funding Award AzAds, the Irish Center for High-End Computing (ICHEC), Enterprise Ireland, and the European Union's H2020 research and innovation programme under Marie Skłodowska-Curie grant agreement 847402 (ID: MF20210297) are acknowledged.

Data availability

The data supporting this article are included in the ESI.† Crystallographic data for **Ph3MVIm-Br** can be accessed from the Cambridge Crystallographic Data Centre (CCDC) as deposition number 2418964.† Modelled polymerizations are included in the Videos entitled Ph3MVlm-Br.mp4, and Ph3MVBlm-Br.mp4.

Conflicts of interest

The authors have no conflicts to declare.

Notes and references

1 P. Pässler, *et al.*, *Chemistry*, Wiley, 2011.
2 M. L. Foo, *et al.*, *J. Am. Chem. Soc.*, 2016, **138**, 3022–3030.
3 G. Verma, *et al.*, *Eur. J. Inorg. Chem.*, 2021, 4498–4507.
4 R. S. Haszeldine, *Science*, 2009, **325**, 1647–1652.
5 X. Suo, *et al.*, *Adv. Mater.*, 2020, **32**, 1907601.
6 S. Mukherjee, *et al.*, *Chem. Commun.*, 2020, **56**, 10419–10441.
7 Y. Peng, *et al.*, *Angew. Chem., Int. Ed.*, 2018, **57**, 10971–10975.
8 S. Kitagawa, *et al.*, *Angew. Chem., Int. Ed.*, 2004, **43**, 2334–2375.
9 S. Mukherjee, *et al.*, *Angew. Chem., Int. Ed.*, 2021, **60**, 10902–10909.
10 X. Cui, *et al.*, *Science*, 2016, **353**, 141–144.
11 Z. Bao, *et al.*, *J. Am. Chem. Soc.*, 2018, **140**, 4596–4603.
12 X. Chen, *et al.*, *Chem. – Eur. J.*, 2024, **30**, e202303580.
13 C. R. Groom, *et al.*, *Acta Crystallogr., Sect. B:Struct. Sci., Cryst. Eng. Mater.*, 2016, **72**, 171–179.
14 T. He, *et al.*, *Acc. Chem. Res.*, 2021, **54**, 3083–3094.
15 Z. Zhang, *et al.*, *J. Am. Chem. Soc.*, 2022, **144**, 14992–14996.
16 W. Zhang, *et al.*, *ACS Nano*, 2019, **13**, 10261–10271.
17 Y. Shao, *et al.*, *ACS Nano*, 2018, **12**, 11704–11710.
18 H. Pan, *et al.*, *Adv. Funct. Mater.*, 2023, **33**, 2214887.
19 C. Gong, *et al.*, *Angew. Chem., Int. Ed.*, 2022, **61**, e202204899.
20 L. Chen, *et al.*, *J. Am. Chem. Soc.*, 2021, **143**, 10243–10249.